*J. Fluid Mech.* (2005), *vol.* 530, *pp.* 353–368. © 2005 Cambridge University Press 
doi:10.1017/S0022112005003769 Printed in the United Kingdom

# Particle image velocimetry measurements of a steam-driven confined turbulent water jet

By RALPH J. E. VAN WISSEN, KOEN R. A. M. SCHREEL AND CEES W. M. VAN DER GELD

Eindhoven University of Technology, Department of Mechanical Engineering, P.O. Box 513, 5600 MB Eindhoven, The Netherlands

(Received 1 June 2004 and in revised form 22 December 2004)

In this paper experiments are reported on a condensing steam jet. Superheated steam is injected at the bottom centre of a cylindrical water vessel, resulting in a turbulent jet with Reynolds numbers varying between $7.9 \times 10^4$ and $18.1 \times 10.4$, depending on the bulk temperature of the water. Near the steam inlet, the flow is two-phase with rapidly condensing steam. Downstream of a development region the jet is essentially single-phase. Using particle image velocimetry in a vertical plane through the central axis, instantaneous velocity fields of the single-phase region have been measured at a rate of 15 Hz. The velocity field in this region is found to be self-similar, i.e. the width of the jet, $r_{1/2}$, increases linearly with increasing distance to the virtual origin, and a Gaussian profile prevails if velocities and distances are properly scaled. The spreading rate is equal to the one usually found in single-phase jets, and temperature independent. The virtual origin of the jet is positioned at a temperature-dependent distance (3–7 nozzle diameters) upstream of the steam inlet, and this distance is shown to correlate with the length of the condensation region. The turbulence intensity is found to be similar to the intensities usually reported for single-phase jets, although full isotropy is only reached at a distance of 15 nozzle diameters from the nozzle. The jet exhibits a slow wobbling motion, which can be attributed to instability of the backflow resulting from the confinement. When the measurements are compensated for this wobble, a slightly smaller spreading rate is obtained, which indicates that unconditional averaging may conceal significant flow structuring.

## 1. Introduction

When fluid is emitted from a circular or ring-shaped orifice into a large space containing stationary fluid, a jet is formed, which has a time-averaged velocity field that is axisymmetric with a basically self-similar velocity profile. The velocity profile and turbulence properties of jets of this type are important because of their application in many operations, e.g. those occurring in combustion, propulsion and in the process industry. Apart from these single-phase jets, a number of applications use condensing jets, in which a saturated or superheated vapour is injected into a liquid. This type of jet can be applied for heating purposes when a high mixing rate is also needed. In this paper an experimental study is presented of the structure of a condensing jet and its velocity field in the condensed region. As a medium, superheated steam injected into subcooled water is chosen.

Non-condensing and single-phase flow jets have been studied thoroughly since the beginning of the previous century. For an extensive overview see e.g. Panchapakesan &

Lumley (1993). The earlier analyses assumed a point source of momentum and focused on a far-field analysis (Tollmien 1926; Monin & Yaglom 1971; Pope 2000). In the last few decades, jets based on a flat-top velocity profile near the nozzle exit have been studied. George (1989) provided an in-depth analysis, and experimental work was performed by Hussein, Capp & George (1994) and Panchapakesan & Lumley (1993). The main focus of these papers was the self-similarity in the far field of these jets and turbulence properties, in particular the validation of higher-order closure models. The far-field self-similarity requires that the flow is dependent only on the total mass and momentum flux, making the effective radius a proper scaling parameter. This effective radius is the radius of a hypothetical jet with mass density equal to that far away from the jet exit, $\rho_\infty$, and with the same initial mass flux and initial momentum flux of the jet. If the inlet mass density, $\rho_0$, is constant, the effective radius is defined as

$$r_\varepsilon = \frac{\sqrt{\dfrac{\rho_0}{\rho_\infty}} \displaystyle\int u(0,r)\,\mathrm{d}A}{\sqrt{\displaystyle\int u^2(0,r)\,\mathrm{d}A}}. \tag{1.1}$$

Here $u(0,r)$ denotes the mean axial velocity component at radial distance $r$ at the jet exit. The exit velocity distribution of fully developed turbulent pipe flow is known (Papadopoulos & Pitts 1999) to yield variations in $r_\varepsilon$ of 3 %. Since the flow in the jet exit in our experiments neither corresponds to pipe flow nor is well-developed, bigger variations might be expected. According to direct numerical simulation (DNS) computations of Boersma, Brethouwer & Nieuwstadt (1998), the coefficients of the self-preserving solutions to the axisymmetric jet equations are dependent on the orifice geometry and other initial conditions. The source velocity profile (top-hat, fully developed pipe flow, etc.) and the source Reynolds number affect the values of these coefficients. It is noted that accounting for the inlet turbulence intensity per unit area, by adapting the definition of the effective radius as was done by Papadopoulos & Pitts (1999), is only useful to obtain the velocity field near the jet exit.

Based on visual observations (Weimer, Faeth & Olson 1973; Chen & Faeth 1982), it is known that a superheated steam jet possesses a condensation region. In this region entrainment rates are high and part of the axial momentum is dissipated. Further downstream, a single-phase jet remains. The properties of this jet are subject of this study. No velocity measurements of steam-driven jets have been found in the literature.

In the self-similar region of a turbulent axisymmetric single-phase jet, the mean axial velocity field, $\overline{u}_z$, is by definition described by the following equation:

$$\overline{u}_z(z,r,0) = U_\mathrm{c}(z) f(\eta), \tag{1.2}$$

where $\eta \overset{\mathrm{def}}{=} r/(z-z_0)$, with $z$ the axial coordinate, taken to be zero at the centre of the actual origin of the jet, $z_0$ the coordinate of the virtual origin and $r$ the coordinate in the radial direction. The function $f(\eta)$ describes the self-similar velocity profile and $U_\mathrm{c}$ is the mean centreline velocity, defined by

$$U_\mathrm{c}(z) \overset{\mathrm{def}}{=} \overline{u}_z(z,0,0). \tag{1.3}$$

Measurements of single-phase jets, see for example Hussein *et al.* (1994), indicate that in the far field $U_c$ is inversely proportional to the distance:

$$U_c = \frac{C_0}{(z - z_0)}, \tag{1.4}$$

with $C_0$ a coefficient that is often written as $u_c(0) \cdot r_\varepsilon / K_u$, with $K_u$ the centreline decay rate (Papadopoulos & Pitts 1999).

Hussein *et al.* (1994) showed that a Gaussian profile for $f(\eta)$ fits most data of single-phase, unbounded jets with high accuracy:

$$f(\eta) = \exp\left(\ln(2)\left(\frac{\eta}{S}\right)^2\right). \tag{1.5}$$

Here $S$ is the spreading rate of the jet defined by

$$S \stackrel{\text{def}}{=} \frac{\mathrm{d}r_{1/2}(z)}{\mathrm{d}z} \tag{1.6}$$

where $r_{1/2}$ is the radius at which the mean velocity is half the centreline velocity, at the same height $z$.

The Reynolds number of a turbulent axisymmetric jet is defined by (Pope 2000)

$$Re \stackrel{\text{def}}{=} r_{1/2}(z) U_c(z) / \nu \tag{1.7}$$

and since self-similarity implies $r_{1/2} \sim z$ and $U_c \sim z^{-1}$, $Re$ is independent of $z$.

In jets, as in any free shear flow, structures are convected through the domain making the velocity field intermittent. A circular jet may have a potential core with velocity fluctuations due to the motion of the coherent structures of ring vortices (Hussain & Zaman 1981). The vortex passing frequency, $f$, can be expressed in terms of the Strouhal number

$$Sr = \frac{f d}{U} \approx 0.3 \tag{1.8}$$

with $d$ the exit diameter and $U$ the exit velocity. Acoustic excitation and vortex pairing may affect this frequency (Han & Goldstein 2003). Measurement of the resulting intermittency is not straightforward. Laser-Doppler velocimetry (LDA) and hot-wire measurements merely yield velocities at one location, but not the instantaneous distribution of velocity and vorticity. PIV permits the measurement of multiple instantaneous flow fields. For this reason PIV has been applied in the present study.

This paper reports results and an analysis of experiments performed with a steam jet originating from a ring-shaped orifice, and condensing in water. In the next section the experimental set-up is described, including the PIV analysis details and error estimates. In § 3 the results are presented and analysed. Velocity field histories are measured in the area where the jet is essentially single phase. Self-similarity of the velocity profile is investigated in the area where the jet diameter is sufficently small with respect to the vessel diameter. Next, the dependence of the velocity profile on bulk water temperature is studied as are the turbulence properties of the jet. Additionally the influence of the confinement is investigated. The paper ends with conclusions.

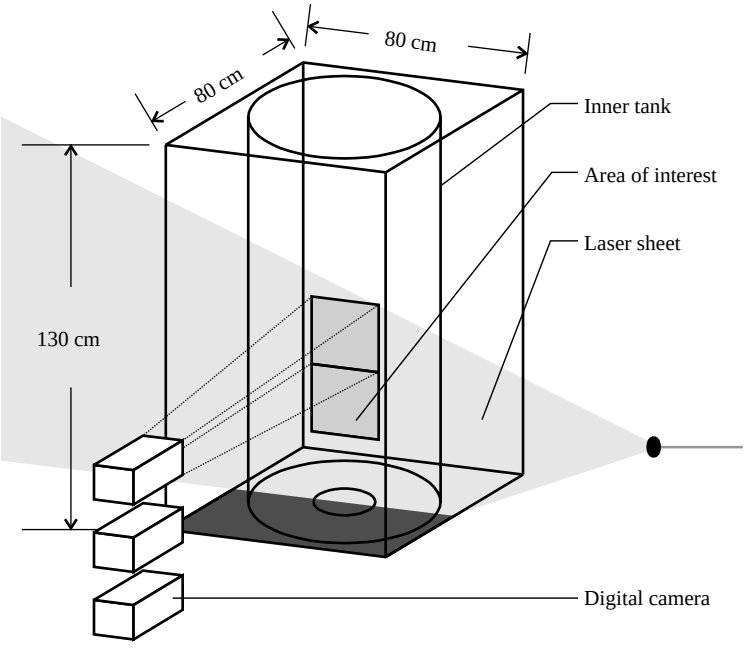


FIGURE 1. Sketch of the measurement set-up.

## 2. Experimental

### 2.1. *Test rig*

Figure 1 shows a schematic of the test set-up. It is essentially a circular symmetric tank with a diameter, $D$, of 65 cm and a height of 130 cm, filled with water. Because of its cylindrical shape, secondary flows caused by corners are absent. Optical distortions are largely compensated by a second, glass tank, with a square cross-section ($80 \times 80$ cm). The space between the two tanks is also filled with water. The cylindrical enclosure is made of Perspex, in order to minimize optical distortions, since the refractive index of Perspex is closer to that of water than glass.

The jet is generated by a ring-shaped injector nozzle with an outer diameter, $d$, of 3 cm and mounted into the base plate. This industrial steam injector is custom-manufactured by Südmo. A positioner from Bürkert (TopControl 8630) is used to operate the nozzle. The nozzle opening can be arbitrarily varied between closed and maximum opening (10 mm), constantly controlled by a PID (Proportional Integration Differentiation) system. The measurements reported in this paper have all been performed with a nozzle opening of 3 mm, inlet steam pressure of 0.3 MPa, and inlet steam temperature of approximately 135 °C. The vessel is filled with water that initially has a homogeneous temperature of about 20 °C. In typically 6 minutes the water is heated to about 60 °C. For $z/d$ in the range 4–14, the $D/r_{1/2}$-ratio is large enough (exceeding 22) in order for the influence of the container walls to have a negligible effect on the velocity field in the core. Further downstream the jet develops into a jet in a confined enclosure. The $z$-direction is opposite to gravity, and the liquid in the vessel has a height of 100 cm.

Temperatures were measured earlier with a rack of 26 thermocouples (Van Wissen *et al.* 2004), and were nearly homogeneously distributed in a vertical plane through the container. It was found that the temperature distribution outside the jet during steam injection is homogeneous within 1 °C. This bulk temperature is measured during

the PIV experiments with only one thermocouple mounted in the upper part of the tank, and is also used to calculate the viscosity of the water. The bulk temperature rises in time at a rate of about $0.11\,^{\circ}\mathrm{C\,s^{-1}}$ typically. Reynolds numbers, based on $r_{1/2}$ (equation (1.7)), are in the range $7.9 \times 10^4$ to $18.1 \times 10^4$ (depending on bulk temperature), which is a somewhat larger Reynolds number range than that of Hussein *et al.* (1994).

If left alone, the gas–liquid interface at the top can be set into violent motion by the jet. The waves will then capture air bubbles in the liquid, which will spoil the PIV recordings. To reduce this surface motion, a Styrodor grid is used which floats on the liquid. The grid can best be described as a 20 cm long flow straightener with a wall thickness of 2 cm and having 150 channels with a cross section of $3 \times 3$ cm. No liquid is removed from the top, and therefore a recirculation flow along the container walls is established. The effect of the confinement by a vessel of the flow due to jet injection at the flat bottom was computed by Jayanti (2001). A recirculating flow was indeed found.

### 2.2. *Optical set-up and PIV analysis*

Descriptions of PIV can be found in the work of Raffel, Willert & Kompenhans (1998) or Westerweel (1993).

The challenge when using PIV in a two-phase system is mainly posed by the lack of transparency. In the present set-up this mostly occurs in the (small) region where the steam condenses, which prohibits measurements at that position. Further downstream, only small (10–100 μm) bubbles of residual air are present. Instead of being detrimental to the image quality, their incidental benefit is that they can be used as tracers together with polyamid seeding in the liquid. It can safely be assumed that these bubbles follow the flow accurately enough despite their density difference with the surrounding liquid. The image contrast between the core region of the jet and the bulk fluid can still be problematic, but this problem is largely solved by optimizing the particle concentration and constantly adjusting the diaphragm of the camera. We used 3 g of 20 μm polyamid particles per tank filling (330 l water).

A Nd:YAG laser (Spectra-Physics PIV-200) is used to illuminate the tracer particles, delivering two pulses of 200 mJ at 15 Hz. Through a system of mirrors and lenses a laser sheet is created at the area of interest. Three digital cameras are used simultaneously in order to capture a large part of the jet. They are focused on an area of observation of $45 \times 15\,\mathrm{cm^2}$, with a light sheet thickness of 2 mm. Each camera has a resolution of $1018 \times 1008$ pixels with 10 bit digitization (Roper Scientific Megaplus ES-1.0 10 bits) and are all equipped with a 75 mm lens. The resulting resolution is 0.15 mm/pixel. The timing of laser and cameras is controlled with an SRS DG535 pulse-delay generator. The photos from each camera are stored real-time to a RAID-0 disk array attached to a computer running the VideoSavant software package. In order to calibrate the positions, a grid of dots in a plane is photographed before each measurement. The absolute positioning of the grid has an accuracy of 0.1 mm. the relative positions of the dots have an accuracy of 0.01 mm.

The PIV analysis is performed by PIV software written in-house using a fixed-interrogation-area algorithm based on the work of Westerweel (1993). The interrogation window used for the PIV analysis is chosen to be $64 \times 64$ pixels. Normally it is desirable to choose the window size as small as possible to increase spatial resolution. In this case, however, the number of erroneous vectors increases with decreasing window size due to the characteristics and problems of the two-phase flow described above. For the spacing between two displacement vectors a distance of 16 pixels is

selected. Although this results in some overlap (75 %) of the interrogation windows, it also results in a large increase in velocity data, which is beneficial for the filtering and interpolation of spurious vectors. For this purpose, the median filter proposed by Westerweel (1994) has been applied. With our settings, this filter compares a velocity component with the median of its 8 closest neighbours. If the deviation between a vector and its local median exceeds 50 %, the vector is replaced by an interpolated value, based on the 24 closest neighbours. Interpolation is only performed after filtering all vectors.

The temperature of the water in the tank is about 20°C initially, but rises due to the heat taken up from the injected steam. Each set of measurements consists of 50 consecutive pairs of photos taken around a certain temperature. After a temperature rise of 5°C a subsequent set is measured. This procedure is then repeated with a fresh tank filling in order to obtain more data per temperature setting.

### 2.3. *Error analysis*

Differences between a measured velocity component, $u_{i,\mathrm{m}}(t)$, and the actual local velocity component, $u_i(t)$, can be due to timing errors, $b_{\Delta t}$, calibration errors, $b_{\mathrm{dist}}$, and errors in the calculation of the displacement vector, $b_{\vec{x}(t)}$:

$$u_{i,\mathrm{m}}(t) = u_i(t) + b_{\Delta t} + b_{\mathrm{dist}} + b_{\vec{x}(t)}. \tag{2.1}$$

Timing errors ($< 10^{-8}$ s) and calibration errors (0.1 mm absolute, 0.01 mm relative) can be considered negligible. Errors in the calculation of the displacement vectors occur in the cross-correlation process. Possible causes are: smoothing of the displacement vector due to the size of the interrogation window, false peak detection due to a large amount of noise and inaccurate peak detection. The influence of the first two error causes have been minimized by optimization of seeding, diaphragm settings and filtering as described above. It is noted that the noise of the measurements at the lower temperatures (25, 30 and 35°C) is higher, due to the higher contrast between the jet and the bulk region in the water. The inaccuracy in the peak detection is normally in the order of 0.1 pixel, but sometimes it appears that the displacement vectors, measured in pixels, tend to take integer values, commonly referred to as 'peak locking'. In our measurements peak locking is due to the fact that the tracer particles (or residual air bubbles) appear as a single pixel on the PIV photos. Therefore, the position of a peak cannot be determined more accurately than one pixel, the absolute error being $\pm 0.5$ pixel. Since this error is unbiased, the average over 50 measurements effectively reduces the error in the average, by a factor 1/7. The error in the average velocity, $\overline{u}$, is approximately 10 % (95 % confidence interval of 50 samples, $\epsilon = 2\sigma/\sqrt{n-1}$, with $\sigma$ the standard deviation and $n$ the number of samples).

The relative error in pressure is approximately 2 %. The nozzle opening is set with a relative error of 2 %. The measurement error of the thermocouples is estimated to be 0.3°C.

## 3. Results and analysis

### 3.1. *Visual observations and PIV results*

In figure 2 a schematic of the jet is presented, as well as a definition of the $r$-direction and axial $z$-direction, opposite to gravity. Steam exits from a ring-shaped nozzle at an angle of 30° with the vertical axis. The core region inside the ring, directly downstream of the nozzle, cannot be observed, but is probably filled with steam.

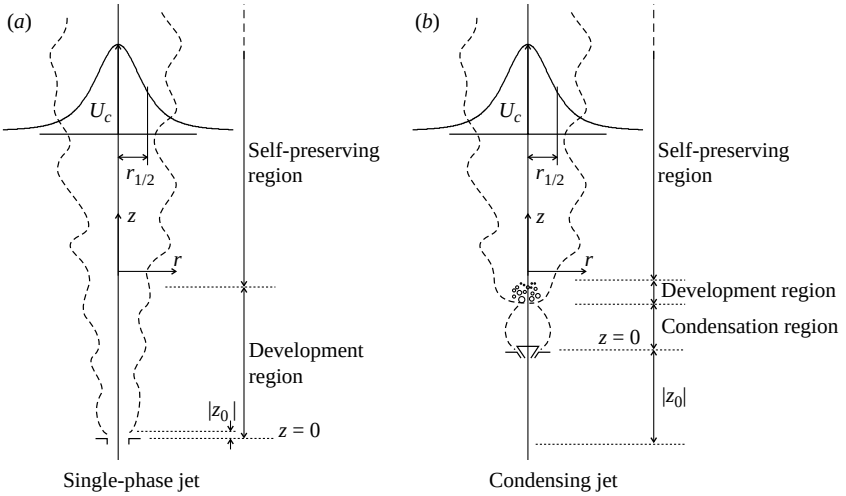


FIGURE 2. Schematic representation of (*a*) a single-phase jet and (*b*) a condensing jet. Drawing is not to scale. For the condensing jet an extra flow regime is distinguished in which the condensation takes place. The condensation gives rise to a large negative value of $z_0$.

Despite of this ring-shaped injection, the outer steam–liquid boundary is similar to that observed by others for steam injection through a circular hole, see Chen & Faeth (1982). The steam–liquid contour has the shape of an onion, widening downstream from the nozzle until some point where rapid contraction to the centreline sets in. The downstream end of the two-phase region is not marked by a sharp boundary between water and a steam–water mixture. Instead, a kind of transition region occurs with bubbles that are partly steam and partly gas. Further downstream, gas residues remain as microscopically small bubbles.

The onion-like shape of the condensation region can be understood by considering linear momentum. Near the nozzle the momentum of the steam has a component in the radial direction, but entrainment of liquid from the core in combination with conservation of mass causes a quick redirection of the flow of injected fluid. Even for fluid–fluid injections this is the case, as has been verified by numerical simulations. In the present two-phase case, this redirection is further promoted by the condensation process in the two-phase volume, and the action of buoyancy.

Downstream of the condensation region, a small development region is distinguished, in which a single-phase jet is established. At a temperature-dependent downstream position a region begins where the jet is single-phase and, as shown below, self-similar. This single-phase jet is the target of the PIV measurements.

The contour plot in figure 3(*d*) shows the vertical component of the time-averaged velocity in the bottom half of the container. In the region below $z = 0.11$ m, data are not reliable due to the high velocity, causing an in-plane particle shift which can be too large to be detected reliably. The contour map of figure 3 is based on an average of 50 measurements in time. The velocity vector spacing is about 2.5 mm. The interrogation window has an equivalent width of 10 mm. For the analysis in the following sections, the average of runs is used (100 velocity maps). Buoyancy effects are negligible in the measurement region, with a Froude number exceeding $10^4$ (Van Wissen *et al.* 2004).

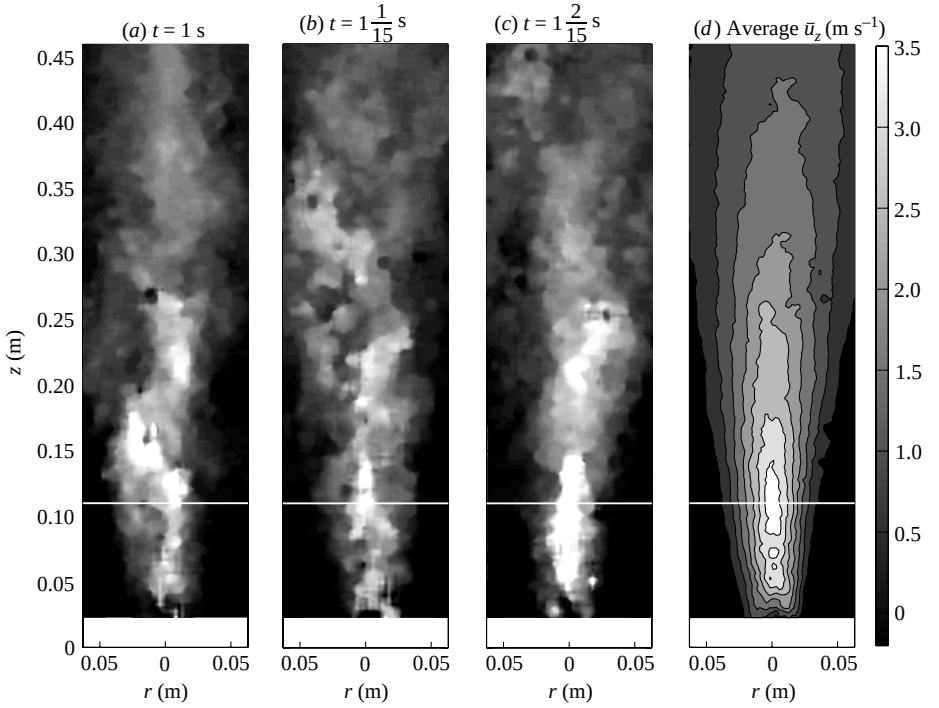


FIGURE 3. (*a–c*) Three instantaneous recordings and (*d*) an average of 50 recordings of the vertical component of the velocity for a bulk water temperature of 55°C. The region below $z = 0.11$ m is not accurate.

### 3.2. *Self-similarity*

To prove self-similarity in the single-phase area, first the centreline velocity, $U_c$, is studied. It is found that $U_c$ complies with equation (1.4), i.e. $U_c$ is linear in $(z - z_0)^{-1}$. For different temperatures, different values of $z_0$ are found, which are given and discussed in the next section. As explained in § 1, this dependency of $U_c$ is characteristic for single-phase jets, and in agreement with much other data, see for example Hussein *et al.* (1994) and Boersma *et al.* (1998).

In figure 4, five iso-velocity-ratio lines are shown on the right-hand side for a bulk temperature of 45°C. For these lines the velocity ratio, $u_z/U_c$, satisfies $u_z/U_c = C$, with $C$ a constant in the range 0.4–0.8. The straight lines are linear fits through the measurements. The points where the lines cross the centreline, $z_0$, are within $\pm 1$ cm from each other. Independent of what the actual expression of $f(\eta)$ is, this shows that the jet is self-similar in this region.

The accuracy of this determination of $z_0$ can be improved by a fitting procedure that uses all data simultaneously and in addition determines the shape of $U_c(z)$ and $f(\eta)$. Before trying to fit the velocity field data for all temperatures, first the field for a fixed temperature was studied. A typical result is presented in figure 5, that shows more than 1200 time-averaged axial velocities, collected at 42 different heights. The self-similarity is obvious. Some functional relations $f(\eta)$, see equation (1.5), taken from the literature, are shown for comparison in figure 5. None of them fits the data at all radial positions. The main reason is that in a relatively small flow region, 15 cm above the steam nozzle, data for the highest two temperatures (55°C and 60°C) clearly show backflow occurring for $r$ in the range $0.07D/2$–$0.12D/2$. For this reason,

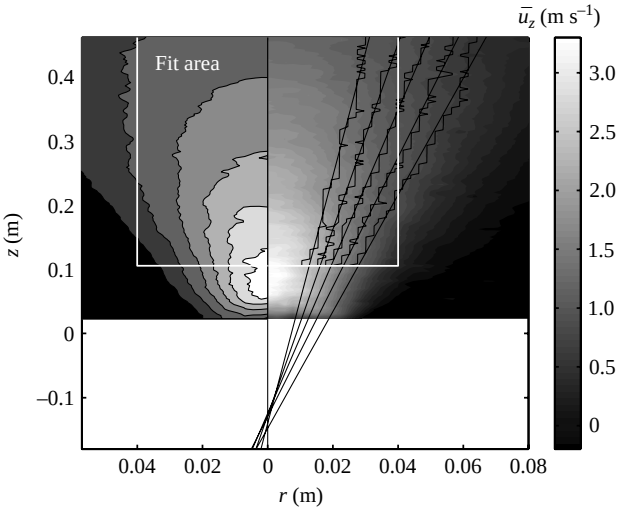


FIGURE 4. Left-hand side: contour plot of the average of the $z$-component of the velocity field for a bulk water temperature of 45 °C. The region below $z = 0.11$ m is inaccurate. The average is constructed of 100 measurements each consisting of 2700 vectors. Right-hand side: lines where $(\overline{u}_z/U_c)$ is constant (0.8, 0.7, 0.6, 0.5, 0.4). The data contained in the area surrounded by the white line are used for fitting the self-similarity profile. The aspect ratio of the axes has deliberately been chosen to enhance the interpretation.

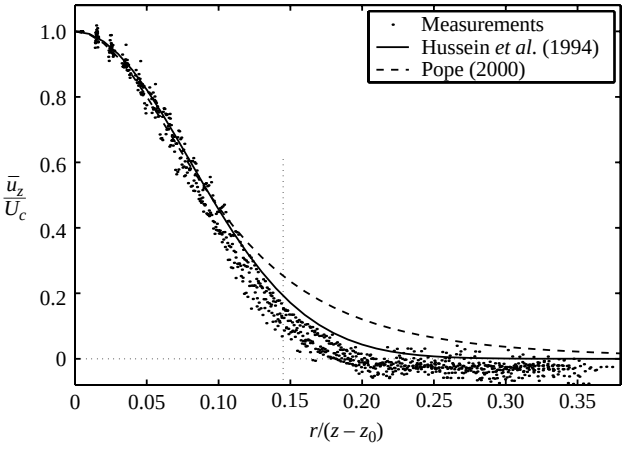


FIGURE 5. Self-similar velocity profiles and our data for bulk water temperature of 55° and heights between 0.106 and 0.205 m.

a limited fitting region has been selected. This region is indicated by the white line in figure 4, and in figure 5 by the vertical dotted line for $z = 0.11$ m. Figure 5 clearly shows that the functional relation given in equation (1.5) and presented by Hussein *et al.* (1994) fits the data in the selected area reasonably well. This observation holds for each bulk water temperature.

### 3.3. *Temperature dependence of the velocity profile*

To study the temperature dependence of the jet profile, the average velocity data obtained at all temperatures have been fitted to equation (1.5). Because of the

| $T_{bulk}$ (°C) | 25 | 30 | 35 | 40 | 45 | 50 | 55 | 60 |
|---|---|---|---|---|---|---|---|---|
| $Re/10^4$ | 7.90 | 8.54 | 9.49 | 10.7 | 12.7 | 14.3 | 16.1 | 18.1 |
| $z_0$ (m) | −0.206(6) | −0.211(6) | −0.147(4) | −0.165(4) | −0.141(3) | −0.134(3) | −0.116(3) | −0.105(3) |
| $C_0$ ($m^2\,s^{-1}$) | 0.751(8) | 0.726(8) | 0.732(7) | 0.752(7) | 0.818(7) | 0.843(7) | 0.883(7) | 0.913(7) |

$$S = 0.0937(7)$$
$$r^2 = 0.86$$
$$F = 1.3 \times 10^4$$

TABLE 1. Fitted coefficients with the error in the last digit within parentheses and fit statistics.

influence of condensation on $z_0$ and $C_0$, these quantities were chosen to be temperature dependent. The fit was done in one run, using 40000 velocity vectors. When the spreading rate ($S$) is fitted as a function of temperature, only little variation and no systematic dependency on temperature is found. Therefore $S$ was taken temperature independent. The required nonlinear least-squares procedure was performed using the Gauss-Newton optimization tool of Matlab. Table 1 shows the results, including estimates for the accuracy of the fit. The correlation coefficient $r^2$ is defined by

$$r^2 = \sum_{i=1}^{N}(\hat{y}_i - \bar{y})^2 \Big/ \sum_{i=1}^{N}(y_i - \bar{y})^2 \tag{3.1}$$

where $N$ is the number of measurements with outcome $y_i$, $\hat{y}_i$ are the corresponding predictions with the fit function, and $\bar{y}$ is the average of all $y_i$. The parameter $F$ is given by

$$F = \frac{r^2}{1 - r^2}\frac{N - k}{k - 1} \tag{3.2}$$

and is an indication of the amount of data used for the fit relative to the number of parameters, $k$.

The value found for $S$ is $0.0937 \pm 0.0007$. All errors indicated are for a 95 % confidence inteval. This value for $S$ is in good agreement with Hussein *et al.* (1994), who found $0.094 \pm 0.001$ (our estimation of error) for hot-wire and LDA measurements of an air jet in an 'infinite' environment ($D/d = 31$), with exhaust to the ambient. Also, the result of Cater & Soria (2002) for a water jet created by a piston is in agreement.

In contrast to most previous results in the literature for non-condensing jets, however, $z_0$ for this condensing jet is always negative. This was also found by Richards & Pitts (1993) for a propane jet created with a pipe. This is caused by the change in mass density during condensation, which compresses the development region, such that the jet seemingly originates from a source upstream of the nozzle. A strong temperature dependence of $z_0$ is observed. This is easily understood from the increase in height of the steam volume above the steam inlet, $x_c$, which has to increase with temperature since the condensation time is longer for higher temperatures. The actual values of $x_c$ are difficult to measure accurately, but are readily estimated from the correlation of Chen & Faeth (1982):

$$\frac{x_c}{d} = 17.8\left(\frac{\rho_0}{\rho_\infty}\right)^{0.5}\left(\frac{h_0 - h_{fs}}{h_{fs} - h_\infty}\right). \tag{3.3}$$

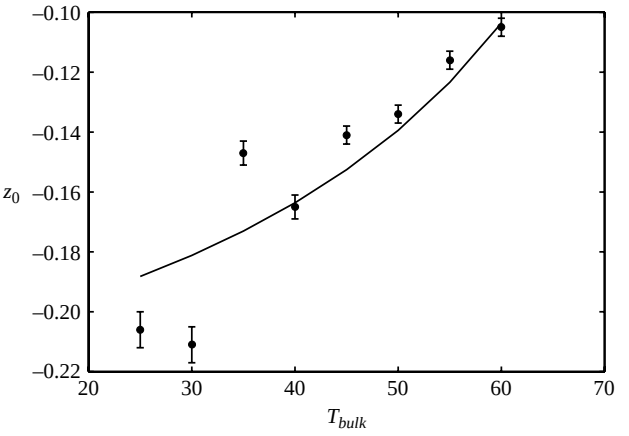


FIGURE 6. Comparison of the temperature dependence of the measured virtual origin ($z_0$) and the temperature dependence of the condensation length (shifted by 0.29 m) according to Chen & Faeth (1982) and given in (3.3).

Typical values at $T_b = 45\,^{\circ}\mathrm{C}$ are: mass density at the steam injector exit, $\rho_0 = 0.705\,\mathrm{kg\,m^{-3}}$, mass density of the ambient water, $\rho_\infty = 990\,\mathrm{kg\,m^{-3}}$, steam enthalpy at the injector exit, $h_0 = 2725\,\mathrm{kJ\,kg^{-1}}$, enthalpy of the saturated liquid, $h_{\mathrm{fs}} = 428.2\,\mathrm{kJ\,kg^{-1}}$, enthalpy of the ambient, $h_\infty = 189\,\mathrm{kJ\,kg^{-1}}$, while the nozzle width $d = 3\,\mathrm{cm}$. Figure 6 shows that $z_0$ varies with temperature in the same way as $x_c$ does. The higher the point where most of the steam is condensed, the higher the point from where the liquid of the jet seemingly originates. The virtual origin of the jet is directly linearly related to the height of the condensing steam part above the steam inlet.

The $C_0$-value is found to increase with increasing bulk temperature, see table 1. The measurements at the lower Reynolds numbers are less accurate, hence the increase can safely be assumed to be homogeneous in the Reynolds range considered. In the usual interpretation of the self-similar region of a single-phase jet, $C_0$ is given by $\bar{u}(0,0)r_\epsilon/K_{\mathrm{u}}$, with $r_\epsilon$ the effective radius and $K_{\mathrm{u}}$ the centreline decay rate, see § 1. The effective radius encompasses the square root of a mass density ratio that varies with temperature. The maximum variations of the square root of the far-field mass density $\rho_\infty$ with temperature (and Reynolds number) are about 1.4 %. This is too small to explain the corresponding increase by about 25 % of $C_0$. However, the effective width of the two-phase part of the jet increases with increasing temperature because of the corresponding decrease of the parameter $B_h = (h_{\mathrm{fs}} - h_\infty)/(h_{\mathrm{fs}} - h_0)$, as demonstrated by Weimer *et al.* (1973). Our observations, and the predictions based on the correlation for the length of the two-phase region, $x_c$, confirm the increase in width with increasing bulk temperature. The actual velocity profile directly downstream of the two-phase region is likely to vary with bulk temperature since the width of the two-phase region does. Analogously to the usual single-phase jets, the decay parameter $K_u/r_\epsilon$ is therefore expected to also vary with temperature; and the same for $C_0$. In this sense the dependence on temperature of $C_0$ is a typical two-phase aspect of a condensing jet.

### 3.4. *Turbulence properties*

In this section, we check whether the turbulence is isotropic, and compare the turbulence intensity level with data for flat-top single phase jets.

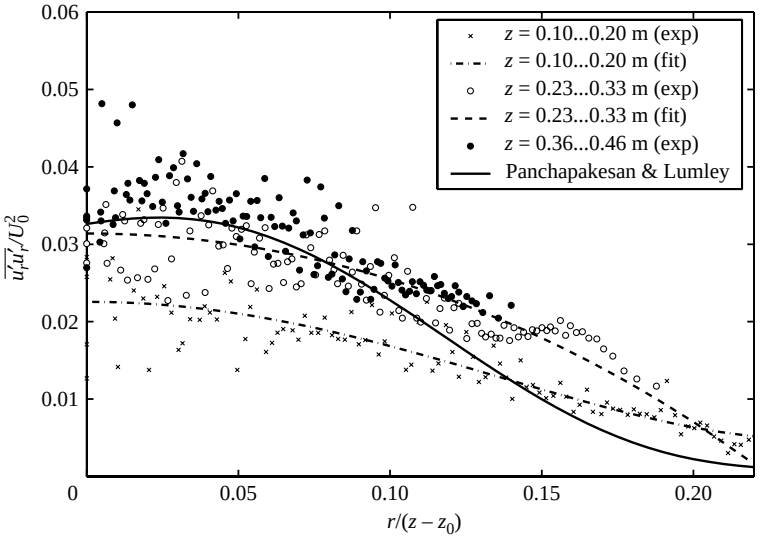


FIGURE 7. Turbulence intensity in the radial direction as a function of normalized radial position for three different $z$-regions at a bulk water temperature of 55°C. The data of Panchapakesan & Lumley (1993) were obtained for values of $30 < z/d < 150$.

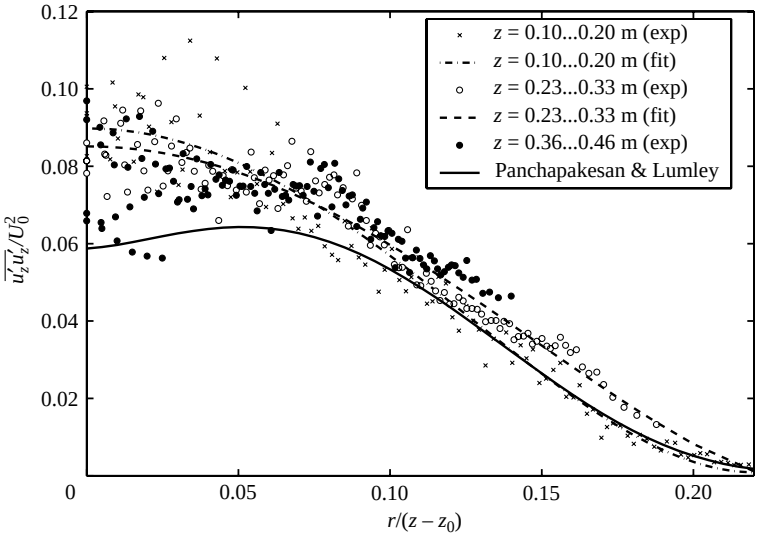


FIGURE 8. Turbulence intensity in the axial direction as a function of normalized radial position for three different $z$-regions at a bulk water temperature of 55°C. The data of Panchapakesan & Lumley (1993) was obtained for values of $30 < z/d < 150$.

The correlations $\overline{u'_r u'_r}$, $\overline{u'_r u'_z}$ and $\overline{u'_z u'_z}$, made dimensionless by $U_c^2$, are shown in figures 7 to 9. Because of the large amount of data from different positions and to eliminate outliers, at each $\eta = r/(z-z_0)$ the medians $\overline{u'_i u'_j}$ of ten values are plotted. For comparison, data Panchapakesan & Lumley (1993) are also presented in figures 7 to 9. Due to the relatively low number (in time) of the average velocities and correlations (100 per average), the accuracy of the time-averages is less than usually obtained with LDA. This explains the spread of the data in figures 7–9. Nevertheless, the measured

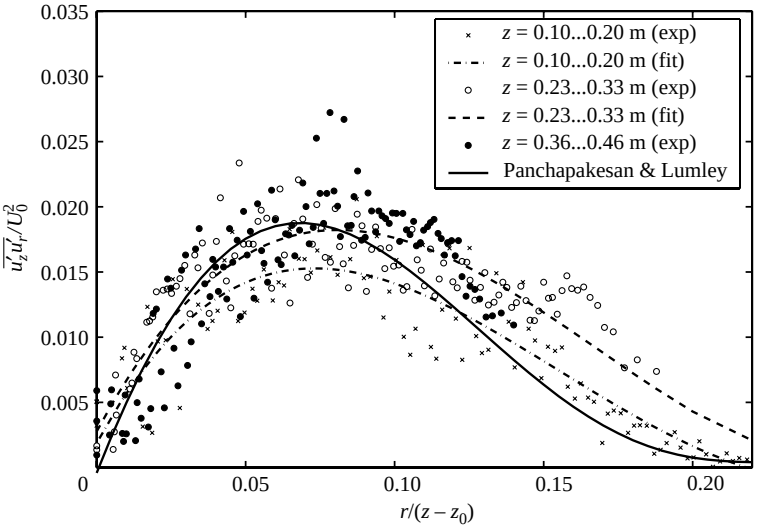


FIGURE 9. The correlation between turbulent fluctuations in the radial and axial direction as a function of normalized radial position for three different $z$-regions at a bulk water temperature of 55 °C. The data of Panchapakesan & Lumley (1993) was obtained for values of $30 < z/d < 150$.

averages show a good agreement with the data of Panchapakesan & Lumley (1993), although they have been obtained for a Reynolds number of $1.1 \times 10^4$. It is even possible to discern some axial development of the correlations: radial component fluctuations increase, and axial velocity fluctuations decrease with increasing distance to the jet exit. Because of these opposing trends, the $\overline{u_z'u_r'}$-correlation is nearly homogeneous. It is concluded that anisotropy is weakly dependent on distance to the virtual origin.

The square roots of $\overline{u_r'u_r'}$ and $\overline{u_z'u_z'}$ yield two RMS values of velocity component fluctuations. A typical RMS value of $u_z$ is $30 \pm 6$ % of $U_c$. That of $u_r$ is $17 \pm 3$ % of $U_c$. Although in correspondence with Panchapakesan & Lumley (1993), our value of the RMS of $u_r$ is 70 % of that found by Hussein *et al.* (1994), and consequently our values of $\overline{u_r'u_z'}$ and $\overline{u_r'u_r'}$ are 70 % and 50 % of those of Hussein *et al.* (1994), respectively.

A possible cause for the differences might be the wall confinement. This is further investigated in the next section. Another reason for discrepancies might be the filtering procedure applied with PIV. As described in § 2.2, the elimination of spurious vectors also induces errors. Velocity fluctuations with a large deviation from the local median are discarded during the removal of spurious vectors. In other words, correctly measured large vectors, that deviate considerably from their neighbours, are deleted. The elimination of these outliers has the effect of decreasing the values of the correlations.

If the temperature is increased, both the mean strain rate, $-\partial \bar{u}_z/\partial r$, and the turbulent production, $P_u = -\overline{u_i'u_j'}\partial \bar{u}_i/\partial x_j$, increase. This temperature dependence is probably related to that of $C_0$, the variation of the virtual origin $z_0$ with temperature, and the variation of the width of the jet with temperature, see § 3.3. The maximum turbulence production rate found is about $150\,\mathrm{m^2\,s^{-3}}$. More details about $P_u$ have been given in a previous paper (Van Wissen *et al.* 2004).

| $T_{bulk}$ (°C) | 25 | 30 | 35 | 40 | 45 | 50 | 55 | 60 |
|---|---|---|---|---|---|---|---|---|
| $Re/10^4$ | 7.90 | 8.54 | 9.49 | 10.7 | 12.7 | 14.3 | 16.1 | 18.1 |
| $z_0$ (m) | −0.172(2) | −0.185(2) | −0.148(2) | −0.145(2) | −0.140(2) | −0.127(1) | −0.121(1) | −0.108(1) |
| $C_0$ ($m^2\,s^{-1}$) | 0.760(4) | 0.742(4) | 0.742(3) | 0.765(3) | 0.827(3) | 0.872(3) | 0.898(3) | 0.925(3) |

$$S = 0.0921(3)$$
$$r^2 = 0.97$$
$$F = 5.4 \times 10^4$$

TABLE 2. Fitted coefficients with the error in the last digit within parentheses and fit statistics for the rotated fit.

### 3.5. *Influence of confinement*

As a consequence of intermittency and instabilities at the jet interface, consecutive PIV measurements, which are taken at a frequency of 15 Hz, exhibit some velocity fluctuations, see the series of three instantaneous recordings in figure 3(*a–c*). The order of magnitude of the frequency of vortex pairing is estimated to be in the range 10–50 Hz. These estimates are based on a Strouhal number in the range of 0.3–0.6, see § 1, a length scale of 3 cm and a velocity scale of $3\,m\,s^{-1}$. If a large number of PIV recordings is put in chronological order and shown as a video, however, the jet appears to be moving from the left to the right, and vice versa at a very low frequency. The resolution in time of the measurements is insufficient to accurately determine the periodicity involved (we measured approximately 1/4 cycle), but frequencies are estimated to be 0.04–0.08 Hz. This low-frequency oscillation may be related to the backflow in the near-wall region, and in particular asymmetry of this backflow with respect to the centre axis of the vessel. This means that the low-frequency oscillation would be related to the confinement of the jet. If so, this would be the first instance where the confinement has been shown to have an effect on the core of the jet.

To explore this idea a little further, the fit procedure has been repeated in a different way. Instead of lumping all velocity data together, the average of each set of 50 velocity fields is first realigned to the central axis. The reasoning behind this is the fact that 50 measurements take a little more than 3 s, which should be long enough to average out the fast fluctuations, but short enough to not feel the recirculation flow instability. The velocity field is realigned by determining the line where the time-averaged velocity is maximal and by rotating the entire average velocity field (by 1° typically), such that this line is vertical.

The fit procedure was repeated on the rotated data, and the results are presented in table 2. Comparison with the fit of the uncorrected data shows the following. There is an occasional shift of the virtual origin of the jet for some temperatures, yielding an even better correspondence with the condensation length prediction of Chen & Faeth (1982). Furthermore, an almost insignificant change of the apparent strength of the jet ($C_0$) is found. The strongest effect, however, is found for the spreading rate of the jet. The value of $S$ is $0.0921 \pm 0.0003$ for the rotated fit, which is smaller than the observed $S = 0.0937 \pm 0.0007$ for the uncorrected fit. This is as expected, since a snapshot of a wobbling jet yields a narrower core than an average over a long period of time.

The question then arises of why the value found for the spreading rate for the uncorrected fit is then in such good correspondence with that for an unconfined jet. This agreement might be coincidental and caused by two compensating effects of

the confinement in our measurements. On the one hand the jet is broadened by the wobbling motion. On the other hand, the backflow causes a slight narrowing of the jet. To be fully conclusive about this, the low-frequency oscillation would need to be resolved with higher accuracy (more data).

## 4. Conclusions

Direct injection of steam in a water vessel is a means of creating a powerful single-phase jet with a virtual origin at about 3–6 nozzle diameters upstream of the actual point of injection. Three regions are identified: a condensation region, a development region, and a single-phase region. The velocity field in the single-phase region of the jet is found to be self-similar, with a spreading rate close to those of isothermal unconfined single-phase jets, measured by others at the corresponding Reynolds number. Although one might expect an influence of the enclosure on the spreading rate due to backflow, a low-frequency precession of the jet centerline might compensate this effect. The Reynolds number, $U_c r_{1/2}/\nu$, increases due to viscosity changes with increasing bulk water temperature. The position of the virtual origin also changes significantly with temperature: it is shown that this change can be directly correlated to the length of the two-phase region of the flow, which is governed by the time needed for condensation of the injected steam. The apparent strength of the jet in the single-phase region ($C_0$) increases with increasing bulk water temperature, as does the turbulent production, for reasons related to changes in the condensation region. This is a typical aspect of a steam-driven jet. The measured intermittencies and turbulent fluctuations correspond to those measured by others, for unconfined single-phase jets.

The financial support of Unilever Research & Development (dr J. Wieringa) is gratefully acknowledged. Dr J. G. M. Kuerten is thanked for stimulating discussions.

## REFERENCES

Boersma, B. J., Brethouwer, G. & Nieuwstadt, F. T. M. 1998 A numerical investigation on the effect of the inflow conditions on the self-similar region of a round jet. *Phys. Fluids* **10**, 899–909.

Cater, J. & Soria, J. 2001 PIV measurements of turbulent jets. *Fourth International Symposium on Particle Image Velocimetry, Göttingen, Germany, September 17–19 2001*, Paper P1019.

Cater, J. & Soria, J. 2002 The evolution of round zero-net-mass-flux jets. *J. Fluid Mech.* **472**, 167–200.

Chen, L.-D. & Faeth, G. M. 1982 Condensation of submerged vapor jets in subcooled liquids. *J. Heat Transfer* **104**, 774–780.

George, W. K. 1989 The self-preservation of turbulent flows and its relation to initial conditions and coherent structures. *Advances in Turbulence*, pp. 39–72. Hemisphere.

Han, B. & Goldstein, R. J. 2003 Instantaneous energy separation in a free jet. Part I. Flow measurement and visualization. *Intl J. Heat Mass Transfer* **46**, 3975–3981.

Hussain, A. K. M. F. & Zaman, K. B. M. Q. 1981 The 'preferred' mode of the axisymmetric jet. *J. Fluid Mech.* **110**, 39–71.

Hussein, H. J., Capp, S. P. & George, W. K. 1994 Velocity measurements in a high-Reynolds-number, momentum-conserving, axisymmetric, turbulent jet. *J. Fluid Mech.* **258**, 31–75.

Jayanti 2001 Hydrodynamics of jet mixing in vessels. *Chem. Engng Sci.* **56**, 193–210.

Monin, A. S. & Yaglom, A. M. 1971 *Statistical Fluid Mechanics: Mechanics of Turbulence*. MIT Press, Boston.

Panchapakesan, N. R. & Lumley, J. L. 1993 Turbulence measurements in axisymmetric jets of air and helium. Part 1. Air jet. *J. Fluid Mech.* **246**, 197–223.

Papadopoulos, G. & Pitts, W. M. 1999 A generic centerline velocity decay curve for initially turbulent axisymmetric jets. *Trans. ASME*: *J. Fluids Engng* **121**, 80–85.

Pitts, W. M. 1991 Reynolds number effects on the mixing behavior of axisymmetric turbulent jets. *Exps. Fluids* **11**, 135–144.

Pope, S. B. 2000 *Turbulent Flows*. Cambridge University Press.

Richards, C. D. & Pitts, W. M. 1993 Global density effects on the self-preservation behaviour of turbulent free jets. *J. Fluid Mech.* **254**, 417–435.

Raffel, M., Willert, C. E. & Kompenhans, J. 1998 *Particle Image Velocimetry: a practical guide*. Springer.

Tollmien, W. 1926 Berechnung turbulenter ausbreitunsvorgange. *Z. Angew. Math. Mech.* **6**, 468–478.

Van Wissen, R. J. E., Schreel, K. R. A. M., Van der Geld, C. W. M. & Wieringa, J. 2004 Turbulence production by a steam-driven jet in a water vessel. *Intl J. Heat Fluid Flow* **25**, 173–179.

Weimer, J. C., Faeth, G. M. & Olson, D. R. 1973 Penetration of vapor jets submerged in subcooled liquids. *AIChE J.* **19**, 552–558.

Westerweel, J. 1993 *Digital Particle Image Velocimetry—Theory and Application*, Delft University Press, Delft.

Westerweel, J. 1994 Efficient detection of spurious vectors in particle image velocimetry data sets. *Exps. Fluids* **16**, 236–247.